



Cite this: *J. Mater. Chem. C*, 2018, **6**, 3538

## One-dimensional conjugated polymer nanomaterials for flexible and stretchable electronics

Yeongjun Lee,  <sup>†a</sup> Huanyu Zhou  <sup>†a</sup> and Tae-Woo Lee  <sup>\*ab</sup>

Stretchable electronics will be essential components of future wearable electronics, biomedical applications, and robotics. Conjugated polymers (CPs) have good mechanical compliance and can be processed via facile solution-based methods; thus, they can be effectively adapted to flexible and stretchable electronics. In addition, the electrical and mechanical properties of CPs can be tuned to satisfy the requirements of various flexible and stretchable next-generation applications. Typically, one effective and simple approach to apply CPs to stretchable electronics is to form one-dimensional (1D) CP nanostructures. This article reviews the recent work on the development of flexible and stretchable 1D CP nanomaterials, including nanofibril networks and printed single nanowires, and their flexible and stretchable applications and then presents some perspectives for future research on 1D CP nanomaterials for flexible and stretchable electronics.

Received 26th December 2017,  
Accepted 7th March 2018

DOI: 10.1039/c7tc05927b

rsc.li/materials-c

### 1. Introduction

Conjugated polymers (CPs) are promising materials for various flexible and stretchable next-generation electronic applications including light-emitting diodes,<sup>1–3</sup> photovoltaics,<sup>4–10</sup> transistors,<sup>11–13</sup> photodetectors,<sup>14</sup> and bio-inspired devices.<sup>15</sup> The molecular

properties of CPs can be easily tuned by modification of the chemical structure and synthesis methods; thus, the requirements for the functional properties of these flexible and stretchable devices can be easily satisfied.<sup>16,17</sup> Moreover, compared to inorganic electronic materials, CPs possess the potential for scalable manufacturing, easy processing, large strain tolerance, and low cost,<sup>18,19</sup> which combinedly lead to a wide range of applications of CPs in flexible and stretchable devices.

Several approaches can be used to develop CP-based flexible and stretchable electronics. Chemical modification of conjugated polymers can increase the mechanical stretchability of organic semiconductor (OSC) films while suppressing the formation of microscale cracks, which degrade the charge-transport property

<sup>a</sup> Department of Materials Science and Engineering, Seoul National University, 1 Gwanak-gu, Seoul 08826, Republic of Korea. E-mail: twlees@snu.ac.kr, taewlees@gmail.com

<sup>b</sup> Institute of Engineering Research, Seoul National University, 1 Gwanak-gu, Seoul 08826, Republic of Korea

<sup>†</sup> These authors contributed equally to this work.



Yeongjun Lee

Yeongjun Lee received his PhD in Materials Science and Engineering from Pohang University of Science and Technology (POSTECH), Korea. He is currently working as a postdoctoral researcher in the Materials Science and Engineering, BK21 PLUS SNU Materials Division for Educating Creative Global Leaders at Seoul National University, Korea. His research focuses on printed electronics, nanowire electronics, and stretchable electronics.



Huanyu Zhou

Huanyu Zhou is currently a PhD candidate in Materials Science and Engineering at Seoul National University, Korea. He received his BS in 2015 and MS in 2016 from Yonsei University. After graduation, he worked in the research institute of an OLED material company as a research engineer for one year. His current research is mainly focused on flexible and stretchable devices based on organic and organic-inorganic hybrid materials.

of an OSC film under large strain.<sup>20–22</sup> Polythiophene-*b*-poly(methylacrylate)-*b*-polythiophene (P3HT-*b*-PMA-*b*-P3HT) triblock copolymers have alternating rubbery and hard segments;<sup>23</sup> herein, a modified triblock copolymer has shown a smaller elastic modulus (6 MPa) and improved elongation at break (>140%).<sup>23</sup> However, because of the insulating PMA segments, it has poor electrical property as compared to pure P3HT.<sup>23</sup> Another approach is to incorporate covalent or dynamic non-covalent cross-linking into the backbone or side chains of conjugated polymers.<sup>15,24,25</sup> Hydrogen bonds can be incorporated into the conjugated polymer, and they can break under strain to release stress before the conjugated polymer crystallites are ruptured; as a result, the stretchability is increased.<sup>15</sup> These intrinsically stretchable OSCs are very promising, but their chemical synthesis method is complicated, and the intrinsic electrical property of conjugated polymers after chemical modification can degrade due to disruption of the conjugation.

Geometric engineering is a possible method to fabricate highly stretchable OSCs by exploiting the characteristics of various structures such as serpentine interconnects and buckled structures.<sup>17,21,26</sup> The serpentine metal or conducting polymer has been used to interconnect bridging organic rigid unit devices on an elastomer substrate.<sup>21</sup> Under large tensile or compressive strain, the interconnections absorb the stress and tend to bend along with the elastomer substrate.<sup>21</sup> This method can achieve high stretchability, but wavy interconnects take a relatively large space and are therefore incompatible with the development of high-density device arrays.<sup>21</sup> Moreover, the fabrication of serpentine metallic interconnects entails complex and costly lithographic patterning. Mechanical buckling of an OSC film can be achieved on pre-stretched elastomer film, such as poly(dimethylsiloxane) (PDMS), *block*-poly(ethylene-*co*-butylene)-*block*-polystyrene (SEBS), Ecoflex or 3M VHB tape.<sup>2,17,21,26</sup> When the applied strain is released, the substrate shrinks and forces the OSC film into a buckled structure, which can then be

stretched to its original length. However, the OSC film is desired to be placed in the neutral mechanical plane to minimize the stress caused by sharp out-of-plane wrinkling; however, the wrinkled film has peaks and valleys at which compression and tension occur;<sup>2,27</sup> therefore it has limitation in device structure design.

To circumvent the difficulty of constructing a dedicated architecture by geometric engineering, methods to develop intrinsically stretchable CPs by exploiting one-dimensional (1D) nanoscale structures are suitable for stretchable applications.<sup>17,21,26</sup> This article mainly reviews the simple approaches to fabricating 1D CP nanofibril (NF) networks and single CP nanowires (NWs) (Fig. 1), and also the wide applications for flexible and stretchable electronics.

## 2. Conjugated polymer nanofibril networks

To achieve high flexibility and stretchability, the structure of CPs can be controlled at the nanoscale. In particular, the formation of CP NF networks in the elastomer matrix can significantly increase the mechanical properties of the blended film. Elastomeric polymer chains at the junction between CP NFs provide for the easy rotating and sliding of CP NFs in the elastomer matrix, while the nanoconfinement effect of CP NFs improves the mechanical stability of CP NFs/elastomer composite films when strain is applied.<sup>28–34</sup> Other than using a CP NFs/elastomer blend, the direct formation of CP NF networks inside the film with the addition of additives can also synergistically improve the electrical and mechanical properties of the film. These CP NFs are attractive conductive fillers with the following benefits: (i) conjugated polymers can produce a percolation network with very long nanofibril bundles, which can help to maintain the electrical pathway under strain, (ii) chemical modification of conjugated polymers can be used to diversely tune the electrical and mechanical properties of the composite films, and (iii) the nanoconfinement effect of CP NFs further increases the mechanical stretchability of composite films.

### 2.1 Conjugated polymer nanofibrils/elastomer blend

Numerous efforts have been devoted to increasing the stretchability of CPs by embedding the CP NFs into an elastomer matrix (Table 1).<sup>28–34</sup> The phase-separation mechanism can achieve this goal while reducing stress accumulation and delaying stress propagation.<sup>33</sup> A CP NFs/elastomer composite was fabricated using a warm solution of poly(3-hexylthiophene) (P3HT); then, amorphous polystyrene blends in a marginal solvent (CH<sub>2</sub>Cl<sub>2</sub>) that had a strongly temperature-dependent solubility for P3HT were spin-coated onto substrates at room temperature (RT).<sup>28</sup> After solidification, the P3HT immediately formed well-interconnected NF networks;<sup>28</sup> although the paper did not report the flexibility or stretchability of the film with the embedded CP NFs, the mechanism of NFs formation was suitable for the fabrication of thin-film transistors (TFTs) on flexible or stretchable substrates.



**Tae-Woo Lee**

*Tae-Woo Lee is an associate professor in Materials Science and Engineering at the Seoul National University, Korea. He received his PhD in Chemical Engineering from the KAIST, Korea, in 2002. He joined Bell Laboratories, USA, as a postdoctoral researcher and worked at Samsung Advanced Institute of Technology as a member of the research staff (2003–2008). He was an associate professor in Materials Science and Engineering at the Pohang University of Science and Technology (POSTECH), Korea, until August 2016.*

*His research focuses on printed electronics based on organic and organic–inorganic hybrid materials for flexible displays, solid-state lightings, and solar-energy-conversion devices.*

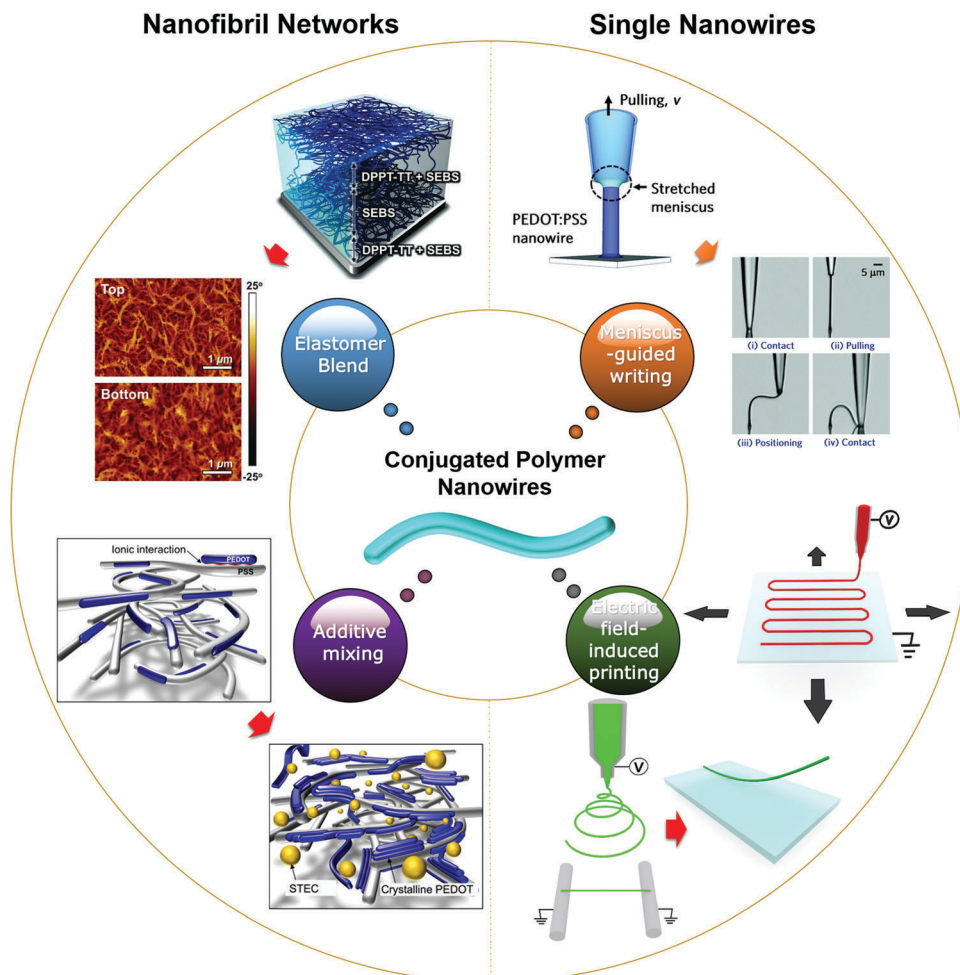


**Fig. 1** Summary of the approaches for fabricating one-dimensional conjugated polymer nanofibril networks, and single nanowires. Elastomer blend: reproduced from ref. 31 with permission. Copyright 2017. American Association for the Advancement of Science. Additive mixing: reproduced from ref. 45 with permission. Copyright 2017. American Association for the Advancement of Science. Electrospinning: reproduced from ref. 54 with permission. Copyright 2018. Wiley-VCH Verlag GmbH & Co. KGaA. Electrohydrodynamic nanowire printing: reproduced from ref. 69 with permission. Copyright 2017. Wiley-VCH Verlag GmbH & Co. KGaA. Meniscus-guided writing: reproduced from ref. 56 with permission. Copyright 2012. American Chemical Society.

**Table 1** Summary of the electrical properties of transistors using CP NF/elastomer composite films

Materials	Pristine ( $\epsilon = 0\%$ )				Under strain			
	$\mu$ ( $\text{cm}^2 \text{V}^{-1} \text{s}^{-1}$ )	$V_{\text{th}}$ (V)	$I_{\text{on}}/I_{\text{off}}$	$\epsilon$ (%)	$\mu$ ( $\text{cm}^2 \text{V}^{-1} \text{s}^{-1}$ )	$V_{\text{th}}$ (V)	$I_{\text{on}}/I_{\text{off}}$	Cycles
P3HT/PS <sup>28</sup> (10 wt%)	$4.0 \times 10^{-3}$	17	$1.0 \times 10^3$	—	—	—	—	—
P3HT/PDMS <sup>29</sup> (10 wt%)	$7.9 \times 10^{-3}$	9.5	$1.6 \times 10^3$	100	$3.7 \times 10^{-4}$	8.3	$1.3 \times 10^3$	—
Pure P3HT <sup>29</sup>	$1.3 \times 10^{-2}$	10.8	$3.3 \times 10^3$	100	$1.7 \times 10^{-5}$	1.7	$3.3 \times 10^2$	—
P3HT/SEBS <sup>30</sup> ( $f_{\text{P3HT}} = 0.01$ )	$5.8 \times 10^{-3}$	$\sim 2$	$1.0 \times 10^5$	50	$1.9 \times 10^{-3}$	—	—	200
DPPT-TT/SEBS <sup>31</sup> (30 wt%)	0.59	—	$\sim 10^5$	100	0.55	—	$\sim 10^5$	1000
P3HT/PDMS <sup>34</sup> (20 wt%)	1.4	-2.56	$5.6 \times 10^3$	50	0.8	-2.45	$\sim 10^2$	—

Another approach to form P3HT NF networks in the PDMS matrix on Si/SiO<sub>2</sub> or PDMS substrate was conducted by slowly cooling the marginal solvent (dichloromethane) from 70 °C to RT (Fig. 2a).<sup>29</sup> A uniform distribution of NF networks embedded in the elastomer could be achieved on the PDMS substrate. In contrast, on the Si/SiO<sub>2</sub> substrate, this process yielded a concentration gradient of P3HT NF networks from the surface of the film to the interface between the Si/SiO<sub>2</sub> substrate

and the PDMS/P3HT NFs composite (Fig. 2a).<sup>29</sup> This gradient formed because the migration of PDMS with a low surface energy to the top surface (air/film interface) is energetically favored, whereas the P3HT NFs migrate to the substrate (film/substrate interface) during spin-coating.<sup>29</sup> Because the density of P3HT NF networks in PDMS is higher near the dielectric interface than in the film, a device with a low P3HT loading (1 wt%, P3HT/PDMS = 1/99) was able to achieve an effective

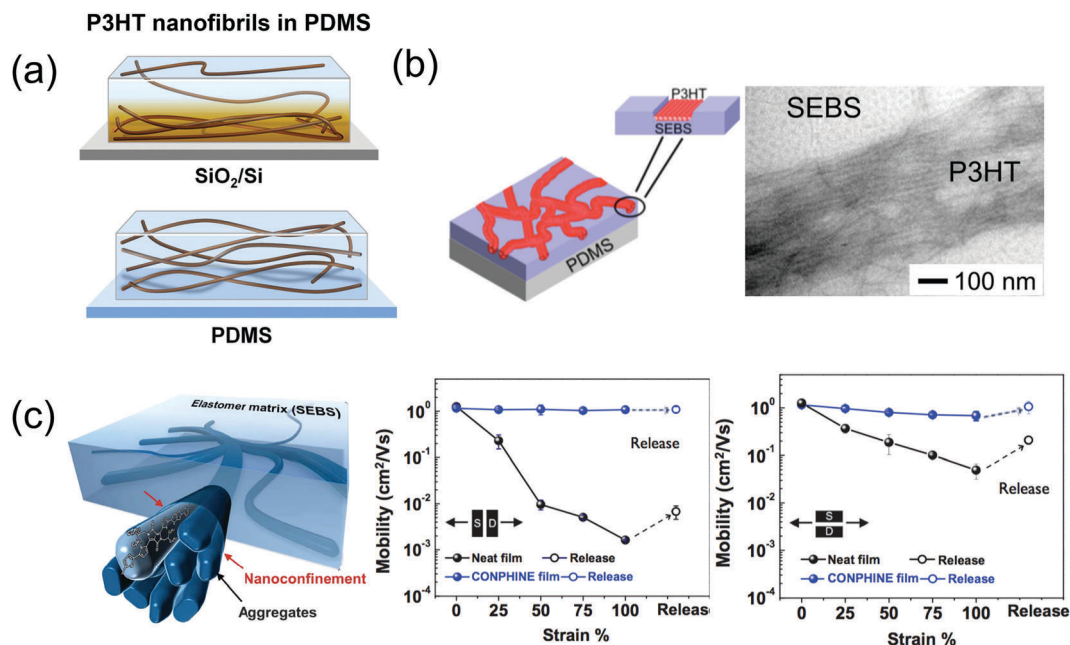


Fig. 2 (a) Schematic of formation of a vertically-graded structure (upper) and uniformly-embedded structure (below) of the P3HT nanofibril networks in the PDMS matrix on a Si or PDMS substrate. Reproduced from ref. 29 with permission. Copyright 2016. Wiley-VCH Verlag GmbH & Co. KGaA. (b) Schematic and TEM image of P3HT nanofibril bundle indented in the SEBS surface. Reproduced from ref. 30 with permission. Copyright 2015. Wiley-VCH Verlag GmbH & Co. KGaA. (c) Schematic of the embedded nanoscale networks of polymer in the SEBS matrix, which can sustain strains parallel and perpendicular to the charge-transport directions. Reproduced from ref. 31 with permission. Copyright 2017. American Association for the Advancement of Science.

charge-transport mobility ( $3.64 \times 10^3 \text{ cm}^2 \text{ V}^{-1} \text{ s}^{-1}$ ) that was comparable to that of devices with pure P3HT NF networks (100 wt%, P3HT/PDMS = 100/0) ( $3.53 \times 10^3 \text{ cm}^2 \text{ V}^{-1} \text{ s}^{-1}$ ).<sup>29</sup> Pure CP NF networks (100 wt%) have strongly-bound junctions between CP NFs, which can be easily broken at relatively small strain (< 30%), but the CP NFs (10 wt%) in the elastomer matrix can be easily rotated and aligned along the stress direction, even at large strain (> 50%); this change occurs because the elastomeric polymer chains weaken bonding at the CP NFs junctions.<sup>29</sup> This flexibility can prevent rupturing of the CP NFs by releasing local stress accumulation.<sup>29</sup> As a result, the carrier mobility  $\mu$  of transistors fabricated using the composite with 10 wt% P3HT NFs was decreased by an order of magnitude after the application of 100% tensile strain, whereas the device with pure P3HT NFs (100 wt%) showed a severe  $\mu$  decrease of three orders of magnitude under the same strain.<sup>29</sup> This result suggests that the incorporation of even small amounts of CP NFs in the elastomer can lead to higher stretchability compared with that of large amounts of CP NFs, because the latter has a high possibility to form tightly-bound junctions, whereas both films have comparable charge-transport mobility in FETs.

P3HT NF networks have also been dispersed in SEBS (Fig. 2b) by using *m*-xylene as the marginal solvent.<sup>30</sup> When the P3HT is not blended with SEBS, a rapid cooling-and-heating process yields phase-separated long NFs in pure P3HT solution at a low temperature and then the long NFs turn into short nanorods as the temperature is increased.<sup>30</sup> However, in P3HT/SEBS blends, the long NFs maintain their length and dispersion in solution throughout the whole cooling-and-heating process.<sup>30</sup>

In transistors fabricated using P3HT NFs/SEBS as the channel material with different P3HT fractions  $0.01 \leq f_{\text{P3HT}} \leq 0.03$ , the device with  $f_{\text{P3HT}} = 0.01$  showed better characteristics than the devices with  $f_{\text{P3HT}} > 0.01$ .<sup>30</sup> The threshold voltage  $V_{\text{th}}$  significantly increased as  $f_{\text{P3HT}}$  was increased from 0.01 to 0.03; this undesired shift was attributed to the easy penetration of moisture and oxygen through the SEBS matrix to the P3HT NF networks.<sup>30</sup> Stretchable transistors with  $f_{\text{P3HT}} = 0.01$  showed stretchability up to 50%.<sup>30</sup> However, an accumulation of mechanical fatigue triggered the formation of cracks, which degraded the on-current and  $V_{\text{th}}$  after 50 cycles of stretching to a strain of 50%.<sup>30</sup>

The improved stretchability of CP NFs in an elastomer matrix can be explained by the nanoconfinement effect (Fig. 2c).<sup>31</sup> Poly(2,5-bis(2-octyldodecyl)-3,6-di(thiophen-2-yl)diketopyrrolo[3,4-*c*]pyrrole-1,4-dione-*alt*-thien[3,2-*b*]thiophene) (DPPT-TT) was chosen as a high- $\mu$  polymer and dispersed in an SEBS elastomer matrix.<sup>31</sup> The nanoconfinement effect suppressed the growth of large crystallites of CP NFs and induced an improvement in the polymer chain dynamics; as a consequence, the mechanical modulus decreased and the mechanical ductility and crack on-set strain of CP increased. The lowered glass transition temperature of the blended film compared to neat CP films also supported the nanoconfinement effect of CP NFs. These changes increase the stretchability of the polymer semiconductor up to 100%, without any cracks, even at the nanoscale.<sup>31</sup> A mixed morphology on the nanoscale was achieved due to the comparable surface energy of polymer semiconductors and SEBS.<sup>31</sup> The film showed biaxial stretchability with a negligible decrease in  $\mu$ , even at 100% parallel or perpendicular

strain applied to the charge-transport direction, with a maximum  $\mu$  of  $1.32 \text{ cm}^2 \text{ V}^{-1} \text{ s}^{-1}$ . Moreover, the high robustness of a transistor with the blended film was demonstrated by applying harsh deformation, such as twisting and poking by a sharp tip, and the transistor still showed stable charge-transport properties.

Various polymer semiconductors have been tested for the nanoconfinement effect, and significant improvements were achieved in stretchability of the polymer semiconductor NFs/SEBS composite without sacrificing its functional properties. Moreover, recently-reported conjugated polymers with chemical modifications, *e.g.*, incorporating rubbery segments, or covalent or dynamic non-covalent cross-linking into the backbone or side chains of conjugated polymers,<sup>15,23,24</sup> were used to form CP NFs or CP NWs to further increase mechanical stability of the composite film. This approach has introduced a new way to fabricate polymer semiconductor/elastomer composites for wearable devices.<sup>31</sup>

## 2.2 Conjugated polymer nanofibrils with additives

In addition, the intrinsic stretchability of CPs could further enhance the stretchability of NF network films. Poly(3,4-ethylenedioxythiophene):poly(styrenesulfonate) (PEDOT:PSS), a well-known conductive CP, with high transparency in the visible range and

superior electric conductivity, has been widely applied for various electronic devices.<sup>35–46</sup> Considering the high solubility of PEDOT:PSS in water, high-quality films can be readily prepared using a conventional wet process, such as spin-coating, ink-jet printing, and electrospinning.<sup>47–49</sup> The solubility mainly originates from the incorporation of hydrophilic PSS with hydrophobic PEDOT. Compared to the long PSS chain, the PEDOT backbone is much shorter and is attached to the long PSS chain *via* Coulombic interactions (Fig. 3a). When the polymeric PEDOT:PSS is dispersed in water, the PEDOT segments form a coiled structure surrounded by PSS chains to minimize the surface energy of PEDOT:PSS.<sup>50</sup> The insulating PSS forms a shell with a thickness of 5–6 nm, which then functions as the energy barrier for the charge transport between PEDOT cores, resulting in the low conductivity of the PEDOT:PSS thin film (Fig. 3a).<sup>43</sup> In addition, considering the PEDOT:PSS thin film with a low fracture strain of  $\sim 5\%$ ,<sup>45</sup> the inclusion of various additives can be an effective route to improve the mechanical stretchability and electrical conductivity of the film (Table 2). Non-ionic surfactants and ionic compounds have been used as additives to improve the electrical conductivity and mechanical stretchability of PEDOT:PSS films. A small amount of non-ionic

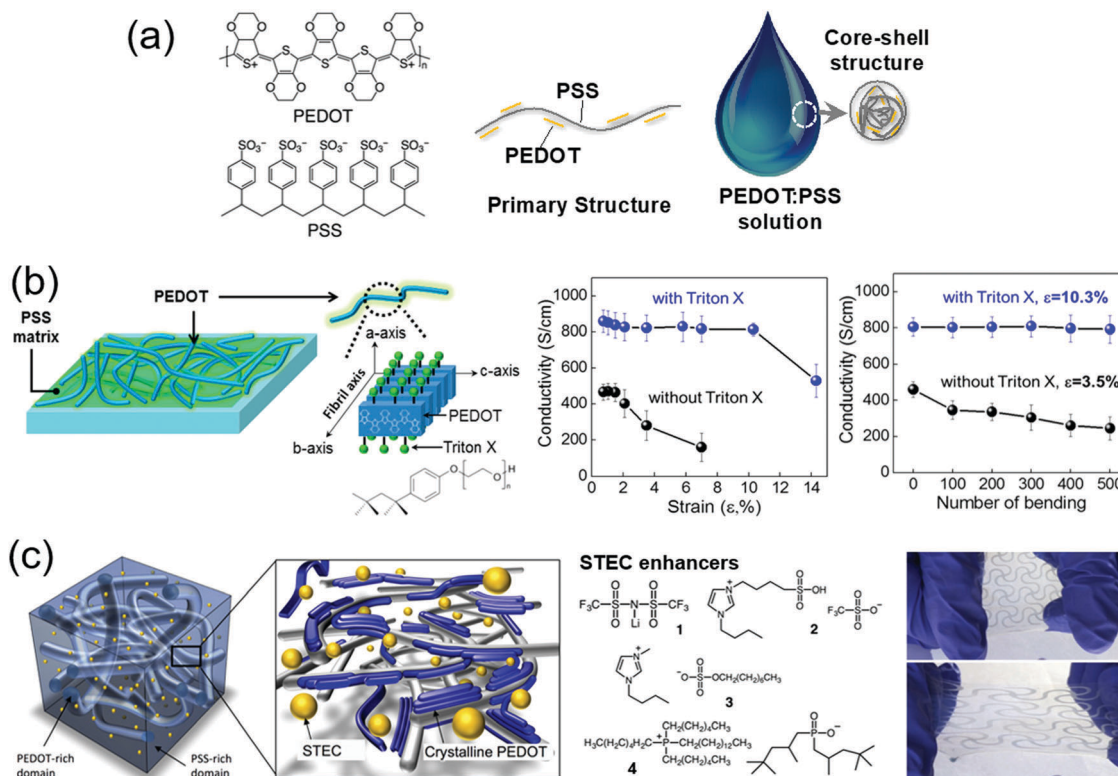


**Fig. 3** (a) Chemical structure and illustration of the primary PEDOT:PSS structure and the core-shell structure in the solution state. Reproduced from ref. 45 with permission. Copyright 2017. American Association for the Advancement of Science. (b) Schematic of a PEDOT:PSS thin film with a surfactant, depicting the molecular packing of PEDOT in the nanofibril and the conductivity of the PEDOT:PSS thin film with or without a surfactant in terms of the bending strain and cycles. Reproduced from ref. 4 with permission. Copyright 2014. American Chemical Society. (c) Schematic of the morphology of a PEDOT:PSS film with STEC enhancers, and the chemical structures of the representative STEC enhancers (1: bis(trifluoromethane) sulfonimide lithium salt, 2: 4-(3-butyl-1-imidazolium)-1-butananesulfonic acid triflate, 3: 1-butyl-3-methylimidazolium octyl sulfate, 4: trihexyltetradecyl phosphonium bis(2,4,4-trimethylpentyl)phosphinate) and a digital image of a patterned PEDOT/STEC film on an SEBS film. Reproduced from ref. 45 with permission. Copyright 2017. American Association for the Advancement of Science.

Table 2 Summary of the representative additives of PEDOT:PSS to achieve high flexibility or stretchability

Types	Additives		Film thickness	Substrate	Functional properties			
	Materials	Amount			Max. $\epsilon$ (%)	Initial $R_s$ or $\sigma$		
Non-ionic surfactant	Zonyl FS-300/DMSO <sup>20,35</sup>	1.0 wt%/5.0 wt%	~ 70 nm	PDMS	188	260 $\Omega \square^{-1}$		
		10.0 wt%/5.0 wt%	~ 150 nm		—	123 $\Omega \square^{-1}$		
		10.0 wt%/10.0 wt%			—	153 $\Omega \square^{-1}$		
	Triton X-100 <sup>4</sup>	1 wt%	40 nm	Glass	10.3	830 S cm <sup>-1</sup>		
Ionic liquid	Li-TFSI <sup>45</sup>	45.5 wt%	~ 200 $\mu$ m	Freestanding	133	608 S cm <sup>-1</sup>		
	BMIS OSU <sup>45</sup>	45.5 wt%			176	288 S cm <sup>-1</sup>		
	EMIM-TFSI <sup>45</sup>	45.5 wt%			71	720 S cm <sup>-1</sup>		
	EMIM-TFSI/Xyl <sup>41</sup>	~ 70 wt%/0.75 wt%			14 $\mu$ m	—	600	407 S cm <sup>-1</sup>
	EMIM-TCB/Capstone <sup>46</sup>	1.0 wt%/1.0 wt%			120 nm	PDMS	50	~ 1000 S cm <sup>-1</sup>

surfactants, such as Triton X-100 and Zonyl FS-300, increased not only the wettability of PEDOT:PSS solution on a hydrophobic surface but also the stretchability of PEDOT:PSS films.<sup>4,40</sup>

The addition of polar solvents in the PEDOT:PSS solution, *e.g.*, dimethyl sulfoxide (DMSO) and ethylene glycol, can improve the conductivity of the resultant films.<sup>38</sup> The combination of non-ionic surfactants and polar solvents can modulate the electrical and mechanical properties of PEDOT:PSS films.<sup>4,40</sup> In the case that ionic compounds are added, both the electrical and mechanical properties of PEDOT:PSS films can be improved, but the amount of ionic additive should be carefully controlled to prevent aggregation caused by strong ionic interaction between PEDOT:PSS and the ionic compounds.<sup>45</sup> The incorporation of a non-ionic surfactant, such as Triton X-100, can improve the flexibility of the film to a bending strain of 10% without significant changes in the conductivity (Fig. 3b).<sup>4</sup> This result may occur because the Triton X-100 facilitates the self-assembly of PEDOT chains to turn into NFs, with a consequent improvement in the mechanical properties.<sup>4</sup> The modulus of the PEDOT:PSS film decreased from 550 MPa to 92 MPa with the addition of 2 wt% of Triton X-100 into the film.<sup>44</sup> The Young's modulus of the PEDOT:PSS film was measured using the buckling method.<sup>44</sup> In addition, the modulus of the film with Triton X-100 further decreased to 80 MPa after a post-fabrication dripping process using methanol to remove the PSS part. This process preferentially removes the Triton X-100-PSS complexes from the film, and yields a decrease in modulus and an increase in conductivity.<sup>44</sup>

Incorporating ionic additives can also achieve highly stretchable and conductive PEDOT:PSS films. Special ionic additives called stretchability and electrical conductivity (STEC) enhancers (Fig. 3c)<sup>45</sup> have good solubility in PEDOT:PSS; the highly acidic anions of the additives dope the PEDOT effectively.<sup>45</sup> Furthermore, the small ionic species cause a charge screening effect that weakens the Coulombic interaction between PEDOT and PSS; as a result the weakened PEDOT is allowed to partially dissociate from the highly coiled PSS and adopt a more planar conformation from a benzoid to quinoid structure, which increases the delocalization of charge carriers and hence the crystallinity and conductivity of PEDOT.<sup>45</sup> The inclusion of ionic additives, as a result, increases the interconnectedness of PEDOT NF structures dispersed in the soft PSS matrix; this change increases the stretchability to > 100% with a conductivity > 4100 S cm<sup>-1</sup>.<sup>45</sup>

### 3. Single conjugated polymer nanowires

Individual single NWs can provide flexible and stretchable electronic devices with nanoscale active channels, without additional subtractive patterning processes. By controlling the chemical composition and morphology of single CP NWs, their mechanical properties can be tuned to meet the requirements of flexible and stretchable electronic devices. To improve the reliability of flexible and stretchable devices based on single CP NWs, position- and alignment-controllable and arbitrarily-long NWs are preferred over short NWs. In this chapter, we review the straightforward and inexpensive direct printing of NWs with stable mechanical and electrical properties by using electrospinning,<sup>51–54</sup> electrohydrodynamic nanowire printing,<sup>55</sup> and three-dimensional (3D) nanoarch printing technologies (Table 3).<sup>56,57</sup>

#### 3.1 Electrospinning

Electrospinning is a facile way to make continuous and ultra-long organic nanowires (or nanofibers; to avoid any confusion caused by terminology similarity between 'nanofiber' and 'nanofibril', the 'nanowire' in this review is referred to as 'nanofiber') networks by a solution process (Fig. 4a). High-molecular-weight binding polymers, such as poly(ethylene oxide) (PEO), polyvinyl alcohol, and poly( $\epsilon$ -caprolactone) (PCL), are generally mixed with CPs to improve their "electrospinnability" by compensating for the relatively low molecular weight of CPs. Because the application of electrospun NWs to electronic devices is advantageous, a large amount of research on electrospun organic or inorganic NW-based electronics has been reported over the last few decades.<sup>51–54,58–67</sup> In particular, a strong electric field improves the molecular chain alignment along the longitudinal direction in the electrospun CP NWs, and therefore the electrical properties of devices based on NWs are usually superior to those of devices based on thin films with the same active material.<sup>52,61</sup> The improvement in molecular alignment, and the crystal packing and ordering in the electrospun NWs was confirmed in UV-vis absorption spectra;<sup>53,60</sup> for example, the maximum absorption wavelength of electrospun CP NWs was red-shifted by 50 nm from that of a CP film due to better  $\pi$ -conjugation.<sup>53</sup> However, the development of CP NW-based flexible and stretchable electronics is still at the early stage despite their promising features.

Table 3 Summary of the recent development in single CP NWs for flexible and stretchable devices

Method	Collectors	Polymers	Jetting formation	Wire diameter	Applications	Max. $\epsilon$ (%)
Electrospinning	Flat collector	P3HT:PCL <sup>51</sup> (mat)	Electrostatic force	$\sim 2.5 \mu\text{m}$	Electrochemical transistors	70
		P3HT:P3DT <sup>52</sup>		$0.1\text{--}3 \mu\text{m}$	Transistors	1.7
	Rotating drum	PQT-12:PEO <sup>53</sup>		$\sim 500 \text{ nm}$	Phototransistors	6.67
		FT4-DPP:PEO <sup>54</sup>		$\sim 695 \text{ nm}$	Transistors	100
Electrohydrodynamic nanowire printing	Parallel electrodes	P3HT:PEO <sup>55,70</sup>		$\sim 300 \text{ nm}$	Transistors, memory	—
		N2200:PEO <sup>69</sup>		$\sim 300 \text{ nm}$	Transistors	—
3D nanoarch printing		PEDOT:PSS <sup>56,82</sup>	Meniscus-pulling	195–495 nm	Interconnects, photoswitches, electrochemical transistors	270
		P3HT-PbS QDs <sup>57</sup>		$\sim 500 \text{ nm}$	Photodetectors	100
		Polypyrrole <sup>81</sup>		100–900 nm	Photoswitches	—

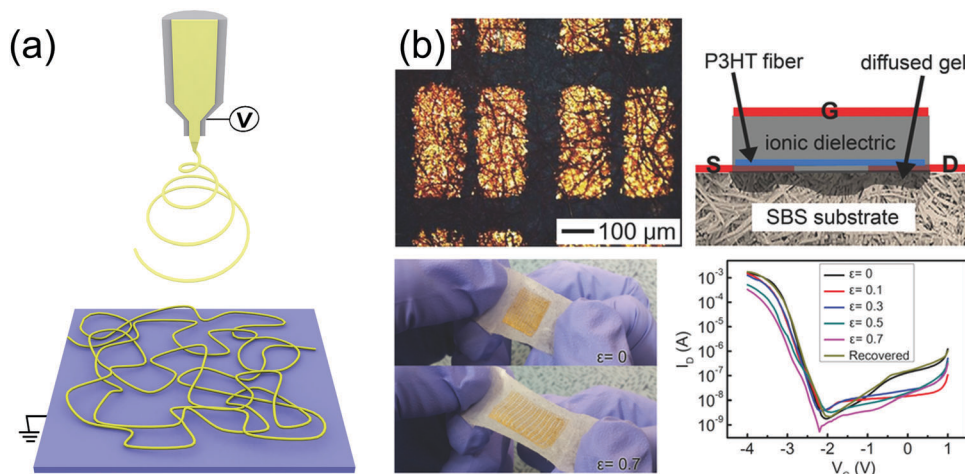


Fig. 4 (a) Schematic of electrospinning. (b) Optical microscope image and schematic of transistors with Au nanosheet S/D electrodes on the SBS nanowire mat and the P3HT wires. Digital image of the device array stretched at a strain rate of 0.7. Transfer curves of the device at different strains. Reproduced from ref. 51 with permission. Copyright 2014. Wiley-VCH Verlag GmbH & Co. KGaA.

Basically, electrospinning produces randomly-oriented NW mats on a grounded flat collector. The curvatures of NWs are large enough to directly connect source and drain (S/D) electrodes, *e.g.*, 50  $\mu\text{m}$ -gap channel of transistors; therefore, the electrical properties of transistors mostly rely on monolithic NWs rather than the percolation of NWs. Moreover, it is difficult for all the nanowires to form a good contact with the bottom S/D electrodes since the later formed nanowires are stacked on top of the initially formed NWs. Despite the difficulty in forming good electrical contact, a highly stretchable and reliable array of polymer transistors with entirely stretchable elements was demonstrated using P3HT:PCL composite wires on a poly(styrene-*b*-butadiene-*b*-styrene) (SBS) electrospun elastomer NW mat substrate ( $\sim 500 \mu\text{m}$  thick) with S/D electrodes made of Au nanosheets ( $\sim 80 \text{ nm}$  thick) (Fig. 4b).<sup>51</sup> Au nanosheet electrodes showed a sheet resistance  $R_S < 5 \Omega \text{ sq}^{-1}$  and excellent stretchability on the SBS NW mat.<sup>51</sup> A UV-cured polyelectrolyte-gel gate dielectric on the electrospun P3HT/PCL wires penetrated through Au nanosheet electrodes and the SBS NW mat, and resulted in an interpenetrated structure, which is a critical requirement to achieve mechanical stability under high tensile strain.<sup>51</sup> With another Au nanosheet ( $\sim 80 \text{ nm}$  thick) on the patterned dielectric gel as

the gate electrode, a stretchable transistor array ( $15 \times 12$ ) was shown to be able to operate reliably at 70% tensile strain and even after 1500 stretching cycles.<sup>51</sup>

Line-by-line arranged single NWs can improve the contact between NWs and bottom S/D electrodes and controllability of the electrical properties of devices could be achieved by adjusting the number of NWs. Electrospun single CP NWs composed of P3HT and poly(3-hexylthiophene) (P3DT) were used as flexible field-effect transistors on a polyethylene terephthalate (PET) substrate with a poly(methyl methacrylate) dielectric layer and a PEDOT:PSS gate electrode.<sup>52</sup> A transistor with a single P3HT:P3DT NW had a field-effect  $\mu = 5.0 \times 10^{-3} \text{ cm}^2 \text{ V}^{-1} \text{ s}^{-1}$ , which exceeded that of film-based devices ( $0.06\text{--}0.07 \times 10^{-3} \text{ cm}^2 \text{ V}^{-1} \text{ s}^{-1}$ ). The single-NW devices maintained electrical charge transport under a bending-induced tensile strain of 1.7% ( $r_B = 5 \text{ mm}$ ) and even after 1000 cycles of bending with the same  $r_B$ .<sup>52</sup>

During the electrospinning process, a rotating drum collector can also be used to align the CP NWs instead of a flat collector.<sup>53</sup> Organic NWs fabricated using a mixture of poly(3,3'-didodecyl-quarterthiophene) (PQT-12) and PEO were aligned onto the drum collector with a rotating speed of 1500 rpm (Fig. 5a).<sup>53</sup> Flexible phototransistors were fabricated on a textile-type PET

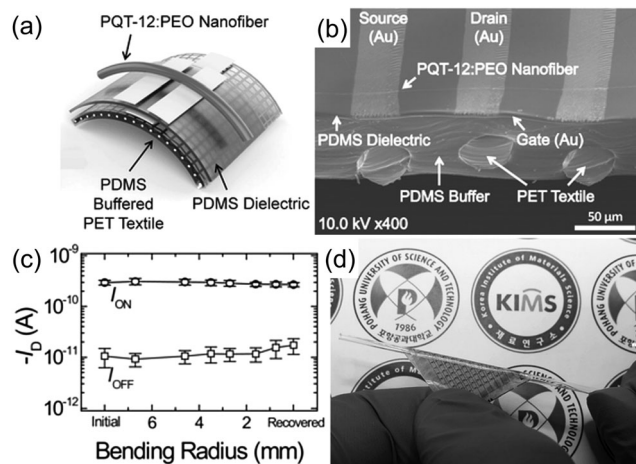


Fig. 5 (a) Schematic and (b) cross-section of PQT-12:PEO nanowire phototransistors. (c) Changes in the on-current and off-current under various bending radii (down to 0.75 mm). (d) An image of phototransistors with a bending radius  $r_B \sim 0.75$  mm. Reproduced from ref. 53 with permission. Copyright 2016. Wiley-VCH Verlag GmbH & Co. KGaA.

and PDMS composite substrate with aligned NWs (Fig. 5b); the devices showed stable electrical characteristics at  $r_B = 0.75$  mm (tensile strain of 6.67%) (Fig. 5c and d).<sup>53</sup> Moreover, after 100 cycles of bending to  $r_B = 2.5$  mm, the on-current of devices decreased by <20%.<sup>53</sup> Compared to a device fabricated using PQT-12:PEO composite film, NW phototransistor showed better photoresponses, possibly because of the large surface-to-volume ratio and high degree of crystallinity of electrospun NWs.<sup>53</sup> High-resolution 10-by-10 phototransistor arrays on a highly-flexible textile-type substrate (Fig. 5d) achieved spatial photosensing mapping under star-shape light illumination by a laser source.<sup>53</sup>

To fabricate stretchable organic NW field-effect transistors, single electrospun CP NWs were achieved by using parallel electrodes, and were then transferred onto elastic polymer substrates (Fig. 6).<sup>54</sup> The NWs consisted of a polymer semiconductor based on fused thiophene diketopyrrolopyrrole (FT4-DPP) combined with PEO, a well-known polymer that shows viscoelasticity during electrospinning.<sup>54</sup> Furthermore, PEO has a low glass transition temperature and low Young's modulus  $E_y$ , and can therefore increase the mechanical ductility of composite NWs by decreasing their  $E_y$ .<sup>54,68</sup> The obtained NWs were continuous after the application of 100% compressive or tensile strain.<sup>54</sup> Under 100% tensile strain, the NWs were fully elongated with an average diameter of 280 nm (before stretching  $\sim 675$  nm).<sup>54</sup> Stretching weakened the  $\pi$ - $\pi$  interactions between the DPP domains in the NWs, so the charge-carrier transport property of the stretched NWs was reduced compared to the pristine NWs.<sup>54</sup> After the strain was released, the NWs were folded with many wrinkles; charge carriers could still move along them.<sup>54</sup> With the application of additional stretching cycles, the wrinkles folded and unfolded repeatedly, so no additional plastic elongation occurred. Geometrically-engineered wavy composite NWs were achieved by applying 100% pre-strain to the elastic substrate without any plastic deformation (Fig. 6a).<sup>54</sup> Therefore, devices

with serpentine NWs showed stable electrical properties under strains of  $\leq 100\%$  (Fig. 6b), and after cyclic stretching. Moreover, stretchable organic NW transistors operated reliably on soft matter that underwent 3D volume changes to mimic biological organs (Fig. 6c),<sup>54</sup> which shows promising properties for future biomedical applications.

Various high-molecular-weight polymers can be used as binding polymers of electrospun CP NWs. In particular, elastomeric polymers, such as PDMS and SEBS, would be promising to increase the stretching stability of CP NWs by suppressing the plastic deformation of NWs. This approach can advance the development of stretchable 1D nanomaterials for soft electronic applications.

### 3.2 Electrohydrodynamic nanowire printing

By decreasing the distance between a tip and a flat collector to  $\leq 1$  cm, NWs can be precisely aligned on a plastic polyimide substrate due to the suppressed instability of a liquid jet under an electric field; this is called the electrohydrodynamic NW printing (ENP) method (Fig. 7a).<sup>55,69-79</sup> ENP can precisely control the location, direction, alignment, patterns, and number of printed NWs in a large area.<sup>55,69-79</sup> Various kinds of NWs, including OSCs, organic insulators, metal oxide semiconductors, metallic conductors, and ferroelectric polymers, and their applications have been demonstrated by ENP.<sup>55,69-79</sup> Highly-aligned P3HT:PEO composite NWs with a core/shell structure were used to fabricate non-volatile ferroelectric transistors on a SiO<sub>2</sub>/Si or polyimide substrate with a ferroelectric poly(vinylidene fluoride-co-trifluoroethylene) (PVDF-TrFE) dielectric (Fig. 7b).<sup>55</sup> The core/shell-structured P3HT:PEO NWs were preferred for electrochemical transistors and synaptic transistors due to the good ion permeability of the PEO shell,<sup>70,71</sup> but in this non-volatile ferroelectric device, excessive positive charges (holes) that had become trapped in the hydrophilic PEO shell caused depolarization of the dipoles at the interface between the NW and the PVDF-TrFE layer, resulting in a decrease in carrier accumulation in the channel, and current retention in the devices.<sup>55</sup> Thermal annealing (180 °C, 10 min) caused changes in the NWs' morphology by transforming the PEO shell into molten PEO islands that were separately located on the P3HT NWs due to the low melting temperature of PEO (65 °C).<sup>55</sup> This configuration induced a direct interface between P3HT and PVDF-TrFE, and thereby increased the current retention time to  $> 10^4$  s, and provided reliable write and erase endurance of  $> 120$  cycles.<sup>55</sup> In this way, flexible non-volatile ferroelectric transistors based on NWs showed consistent two-state non-volatile characteristics and consistent properties after bending for  $> 1000$  cycles to  $r_B = 5.8$  mm (Fig. 7c).<sup>55</sup>

### 3.3 3D Nanoarch printing

3D micro- and nanoarch can provide a margin for mechanical deformation of the device for stretching. Not only have metallic 3D architectures by continuous direct ink writing<sup>80</sup> and drop-on-demand electrohydrodynamic jet printing been demonstrated,<sup>81</sup> but also 3D freestanding single CP NW arches by meniscus-guided direct writing.<sup>56,57,82-85</sup> The nozzle tip is moved close enough to

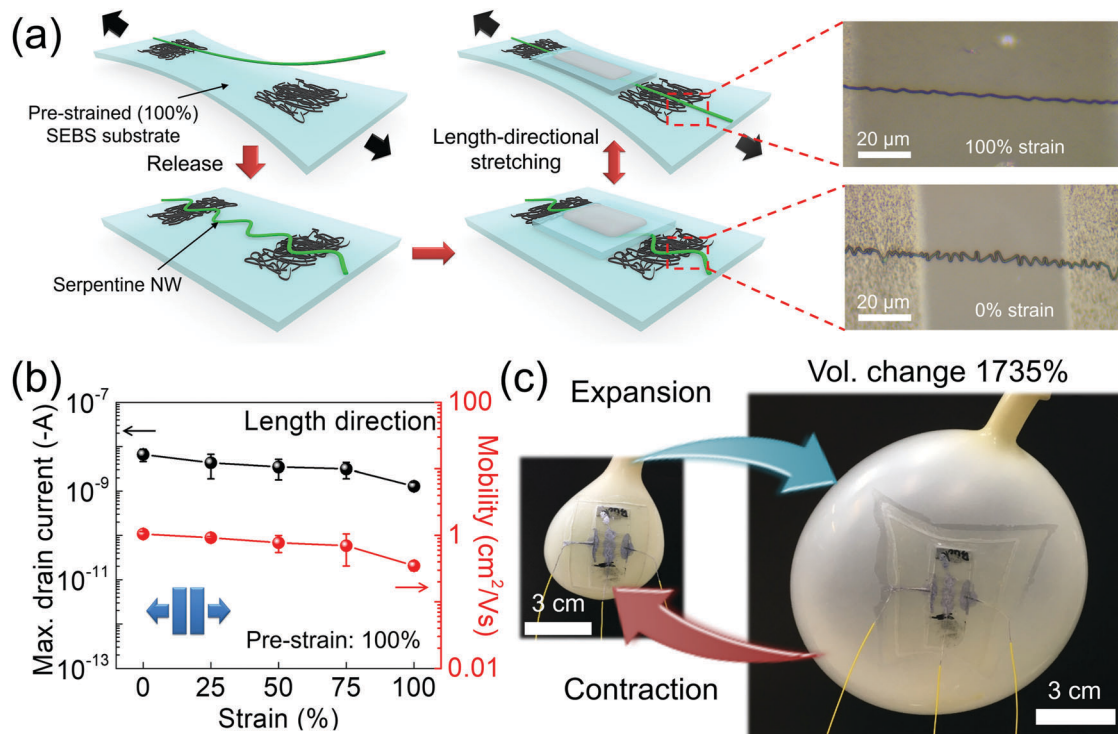


Fig. 6 (a) Schematic of the fabrication process of deformable field-effect transistors with serpentine FT4-DPP:PEO nanowires (pre-strain: 100%) and an SEBS dielectric. Optical microscope images of the serpentine FT4-DPP:PEO nanowires before and after stretching. (b) Carrier mobility and maximum drain current of deformable field-effect transistors with serpentine FT4-DPP:PEO nanowires (pre-strain: 100%) under various strains. (c) Digital images of a deformable field-effect transistors with serpentine FT4-DPP:PEO nanowires mounted on the dynamic surface of a pulsating balloon. Reproduced from ref. 54 with permission. Copyright 2018. Wiley-VCH Verlag GmbH & Co. KGaA.

the substrate to allow a gentle contact with the droplet, and is then pulled away vertically to stretch the liquid meniscus (Fig. 8a).<sup>56</sup> Then, the nozzle is moved to a desired location, at which the nozzle tip is again moved close enough to the substrate to achieve a second soft touch of the liquid to the substrate. During the liquid meniscus stretching, the solvent evaporates and arch-shaped NWs are produced. The diameter of the PEDOT:PSS NWs was controlled from 495 to 195 nm by adjusting the pulling speed of the meniscus from 25.0 to 375 μm s<sup>-1</sup>.<sup>56</sup> The maximum stretching range of NWs depends on the ratio of the arc length  $l_a$  of NW and the planar distance  $l_0$  between the ends of the unstretched NW (Fig. 8b).<sup>56</sup> The  $l_a/l_0$  ratios were controlled up to 4.2, and yielded a maximum stretching range of 270%, which was much higher than the inherent mechanical fracture strain of PEDOT:PSS (~5%).<sup>56</sup> The nanoarch PEDOT:PSS NWs were used in stretchable photo-switches and electrochemical transistors that showed stable functional properties under a strain of >100%.<sup>56</sup> In addition, LEDs fabricated with the stretchable interconnections allowed 270% stretching without a noticeable change in the current-voltage characteristics (Fig. 8c).<sup>56</sup> Stretchable NW photodetectors based on meniscus-guided single-PbS QD-P3HT NWs (radius ~ 250 nm,  $l_a$  ~ 50 μm) absorbed a wide range of light wavelengths from UV to IR with a fast response time (0.11 to 0.58 s) as a result of the photo-induced charge transfer from QDs to P3HT and due to the Schottky diode behavior

(Au/PbS QDs-P3HT NW/Al).<sup>57</sup> NW photodetector arrays fabricated on the PDMS substrate showed no degradation of sensitivity after 100 cycles with 100% tensile strain (Fig. 8d).<sup>57</sup>

## 4. Perspectives

Recent progress in the development of flexible and stretchable electronic devices based on one-dimensional CP nanomaterials was reviewed. One-dimensional CP nanomaterials are soft and flexible, so they are becoming promising components of flexible and stretchable devices for wearable electronics and implantable biomedical applications. In particular, the excellent mechanical stability of CP NFs has stimulated much research on stretchable films in which CP NFs are entangled. Single CP NWs themselves can be used as high-resolution nanoelectronic materials; this trait can eliminate the need for additional tedious lithography-based patterning.

Reported transistors and interconnections based on CP nanomaterials can be driven to a large tensile strength (~100%) without significant degradation, but further development is still possible in the future: by controlling  $E_g$  and the charge-transport properties of the CPs by applying backbone- and side chain-engineering or chemical doping, the mechanical and electrical properties of both network films and single NWs can be further improved, thereby providing a wide range of control over their properties.

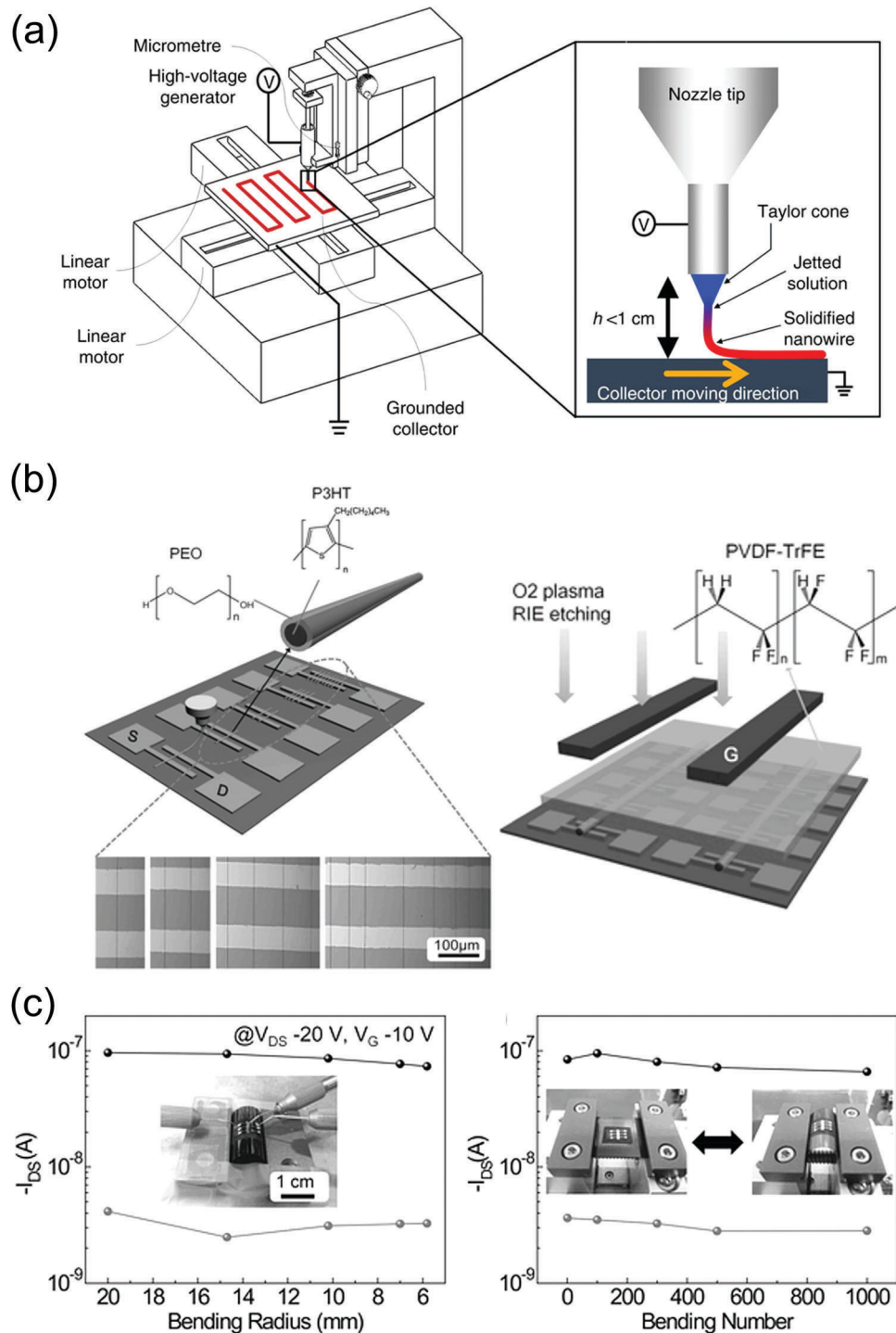


Fig. 7 (a) Schematic of the electrohydrodynamic nanowire printing method. Reproduced from ref. 70 with permission. Copyright 2013. Nature Publishing Group. (b) Schematic illustration of the fabrication process for the non-volatile ferroelectric transistor with aligned P3HT:PEO nanowires and a ferroelectric PVDF-TrFE insulator. (c) 'On' and 'off' currents of a non-volatile ferroelectric transistor on a flexible substrate as a function of  $r_B$  and bending cycles at  $r_B = 5.8$  mm. Reproduced from ref. 55 with permission. Copyright 2014. Wiley-VCH Verlag GmbH & Co. KGaA.

One-dimensional CP nanomaterials can also be modified by geometric engineering, which is advantageous for flexible and stretchable electronic devices. In addition, using an elastic matrix of elastomers, hydrogels, or organogels with a very low  $E_y$ , might enable improvements in stretchability and

introduce additional functions, such as self-healing. These improvements in the electrical properties and mechanical stability of the one-dimensional CP nanomaterials will provide a promising strategy to develop future wearable and implantable devices.

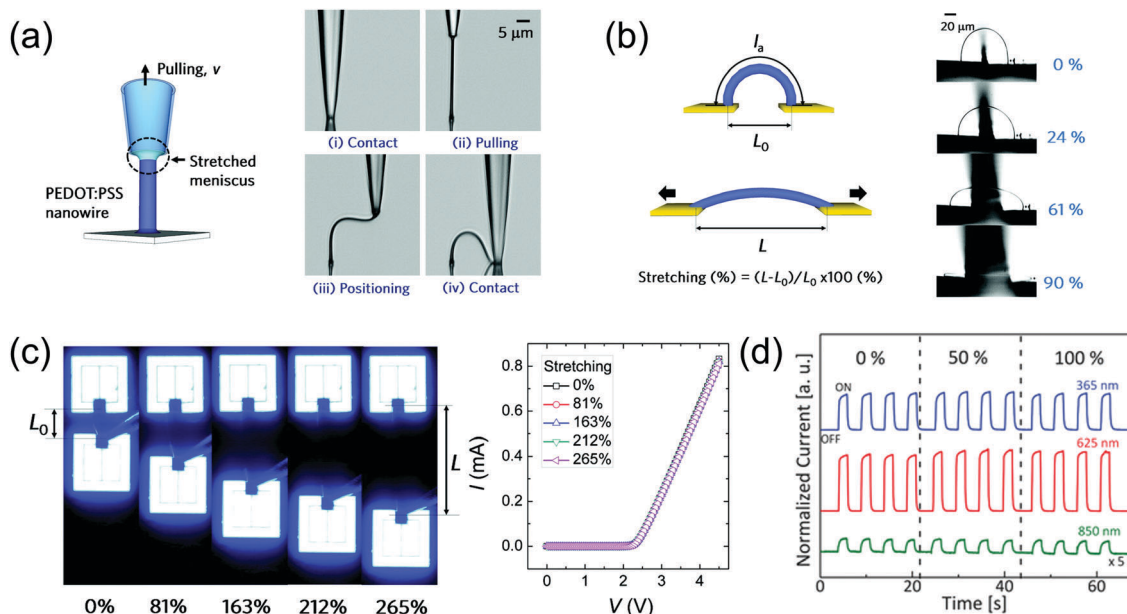


Fig. 8 (a) Schematic and optical images of the formation of a PEDOT:PSS nanowire. (b) Schematic and optical micrographs of the stretching test of the PEDOT:PSS nanoarch up to  $\sim 90\%$ . (c) Optical micrographs and current micrograph of LEDs connected by the PEDOT:PSS nanoarch under stretching up to 265%. Reproduced from ref. 56 with permission. Copyright 2012. American Chemical Society. (d) UV-IR photoresponse of the PbS QD-P3HT nanowire photodetectors during stretching of up to 100%. Reproduced from ref. 57 with permission. Copyright 2015. Wiley-VCH Verlag GmbH & Co. KGaA.

## Conflicts of interest

There are no conflicts to declare.

## Acknowledgements

This work was supported by Creative-Pioneering Researchers Program through Seoul National University (SNU). This work was also supported by the National Research Foundation of Korea (NRF) grant funded by the Korea government (Ministry of Science, ICT & Future Planning) (NRF-2016R1A3B1908431).

## Notes and references

- J. Liang, L. Li, X. Niu, Z. Yu and Q. Pei, *Nat. Photonics*, 2013, **7**, 817–824.
- M. S. White, M. Kaltenbrunner, E. D. Glowacki, K. Gutnichenko, G. Kettlgruber, I. Graz, S. Aazou, C. Ulbricht, D. A. M. Egbe, M. C. Miron, Z. Major, M. C. Scharber, T. Sekitani, T. Someya, S. Bauer and N. S. Sariciftci, *Nat. Photonics*, 2013, **7**, 811–816.
- H.-K. Seo, M.-H. Park, Y.-H. Kim, S.-J. Kwon, S.-H. Jeong and T.-W. Lee, *ACS Appl. Mater. Interfaces*, 2016, **8**, 14725–14731.
- J. Y. Oh, M. Shin, J. B. Lee, J.-H. Ahn, H. K. Baik and U. Jeong, *ACS Appl. Mater. Interfaces*, 2014, **6**, 6954–6961.
- H. Kwon, J. Ham, D. Y. Kim, S. J. Oh, S. Lee, S. H. Oh, E. F. Schubert, K. G. Lim, T. W. Lee, S. Kim, J. L. Lee and J. K. Kim, *Adv. Energy Mater.*, 2014, **4**, 1301566.
- G. Li, R. Zhu and Y. Yang, *Nat. Photonics*, 2012, **6**, 153–161.
- G. Li, V. Shrotriya, J. Huang, Y. Yao, T. Moriarty, K. Emery and Y. Yang, *Nat. Mater.*, 2005, **4**, 864–868.
- H. Kim, S.-H. Bae, T.-H. Han, K.-G. Lim, J.-H. Ahn and T.-W. Lee, *Nanotechnology*, 2014, **25**, 014012.
- H. Kim, J. Byun, S.-H. Bae, T. Ahmed, J.-X. Zhu, S.-J. Kwon, Y. Lee, S.-Y. Min, C. Wolf, H.-K. Seo, J.-H. Ahn and T.-W. Lee, *Adv. Energy Mater.*, 2016, **6**, 1600172.
- S.-H. Bae, H. Zhao, Y.-T. Hsieh, L. Zuo, N. De Marco, Y. S. Rim, G. Li and Y. Yang, *Chem*, 2016, **1**, 197–219.
- G. Schwartz, B. C.-K. Tee, J. Mei, A. L. Appleton, D. H. Kim, H. Wang and Z. Bao, *Nat. Commun.*, 2013, **4**, 1859.
- J. Lee, A. R. Han, H. Yu, T. J. Shin, C. Yang and J. H. Oh, *J. Am. Chem. Soc.*, 2013, **135**, 9540–9547.
- G. Kim, S. J. Kang, G. K. Dutta, Y. K. Han, T. J. Shin, Y. Y. Noh and C. Yang, *J. Am. Chem. Soc.*, 2014, **136**, 9477–9483.
- T. Yokota, P. Zalar, M. Kaltenbrunner, H. Jinno, N. Matsuhisa, H. Kitanosako, Y. Tachibana, W. Yukita, M. Koizumi and T. Someya, *Sci. Adv.*, 2016, **2**, e1501856.
- J. Y. Oh, S. Rondeau-Gagné, Y.-C. Chiu, A. Chortos, F. Lissel, G.-J. N. Wang, B. C. Schroeder, T. Kurosawa, J. Lopez, T. Katsumata, J. Xu, C. Zhu, X. Gu, W.-G. Bae, Y. Kim, L. Jin, J. W. Chung, J. B.-H. Tok and Z. Bao, *Nature*, 2016, **539**, 411–415.
- J. S. Kim, J. H. Kim, W. Lee, H. Yu, H. J. Kim, I. Song, M. Shin, J. H. Oh, U. Jeong, T. S. Kim and B. J. Kim, *Macromolecules*, 2015, **48**, 4339–4346.
- S. E. Root, S. Savagatrup, A. D. Printz, D. Rodriguez and D. J. Lipomi, *Chem. Rev.*, 2017, **117**, 6467–6499.
- R. R. Søndergaard, M. Hösel and F. C. Krebs, *J. Polym. Sci., Part B: Polym. Phys.*, 2013, **51**, 16–34.
- B. Sun, Y.-Z. Long, Z.-J. Chen, S.-L. Liu, H.-D. Zhang, J.-C. Zhang and W.-P. Han, *J. Mater. Chem. C*, 2014, **2**, 1209–1219.

- 20 D. J. Lipomi, J. A. Lee, M. Vosgueritchian, B. C.-K. Tee, J. A. Bolander and Z. Bao, *Chem. Mater.*, 2012, **24**, 373–382.
- 21 Y. Lee, M. Shin, K. Thiyagarajan and U. Jeong, *Macromolecules*, 2016, **49**, 433–444.
- 22 B. Sarkar, D. K. Satapathy and M. Jaiswal, *Soft Matter*, 2017, **13**, 5437–5444.
- 23 R. Peng, B. Pang, D. Hu, M. Chen, G. Zhang, X. Wang, H. Lu, K. Cho and L. Qiu, *J. Mater. Chem. C*, 2015, **3**, 3599–3606.
- 24 G.-J. N. Wang, L. Shaw, J. Xu, T. Kurosawa, B. C. Schroeder, J. Y. Oh, S. J. Benight and Z. Bao, *Adv. Funct. Mater.*, 2016, **26**, 7254–7262.
- 25 H.-C. Wu, S. J. Benight, A. Chortos, W.-Y. Lee, J. Mei, J. W. F. To, C. Lu, M. He, J. B. H. Tok, W.-C. Chen and Z. Bao, *Chem. Mater.*, 2014, **26**, 4544–4551.
- 26 S. Gong and W. Cheng, *Adv. Electron. Mater.*, 2017, **3**, 1600314.
- 27 M. Kaltenbrunner, T. Sekitani, J. Reeder, T. Yokota, K. Kuribara, T. Tokuhara, M. Drack, R. Schwödiauer, I. Graz, S. Bauer-Gogonea, S. Bauer and T. Someya, *Nature*, 2013, **499**, 458–463.
- 28 L. Qiu, W. H. Lee, X. Wang, J. S. Kim, J. A. Lim, D. Kwak, S. Lee and K. Cho, *Adv. Mater.*, 2009, **21**, 1349–1353.
- 29 E. Song, B. Kang, H. H. Choi, D. H. Sin, H. Lee, W. H. Lee and K. Cho, *Adv. Electron. Mater.*, 2016, **2**, 1500250.
- 30 M. Shin, J. Y. Oh, K.-E. Byun, Y.-J. Lee, B. Kim, H.-K. Baik, J.-J. Park and U. Jeong, *Adv. Mater.*, 2015, **27**, 1255–1261.
- 31 J. Xu, S. Wang, G.-J. N. Wang, C. Zhu, S. Luo, L. Jin, X. Gu, S. Chen, V. R. Feig, J. W. F. To, S. Rondeau-Gagné, J. Park, B. C. Schroeder, C. Lu, J. Y. Oh, Y. Wang, Y. Kim, H. Yan, R. Sinclair, D. Zhou, G. Xue, B. Murmann, C. Linder, W. Cai, J. B.-H. Tok, J. W. Chung and Z. Bao, *Science*, 2017, **355**, 59–64.
- 32 S. B. Jo, W. H. Lee, L. Qiu and K. Cho, *J. Mater. Chem.*, 2012, **22**, 4244–4260.
- 33 K. Thiyagarajan and U. Jeong, *MRS Bull.*, 2017, **42**, 98–102.
- 34 H.-J. Kim, K. Sim, A. Thukral and C. Yu, *Sci. Adv.*, 2017, **3**, e1701114.
- 35 S. Savagatrup, E. Chan, S. M. Renteria-Garcia, A. D. Printz, A. V. Zaretski, T. F. O'Connor, D. Rodriguez, E. Valle and D. J. Lipomi, *Adv. Funct. Mater.*, 2015, **25**, 427–436.
- 36 S. Jeong, S. Woo, T. Han, M. Park, H. Cho, Y.-H. Kim, H. Cho, H. Kim, S. Yoo and T. Lee, *NPG Asia Mater.*, 2017, **9**, e411.
- 37 N. Kim, S. Kee, S. H. Lee, B. H. Lee, Y. H. Kahng, Y. Jo, B. Kim and K. Lee, *Adv. Mater.*, 2014, **26**, 2268–2272.
- 38 Y. H. Kim, C. Sachse, M. L. Machala, C. May, L. Müller-Meskamp and K. Leo, *Adv. Funct. Mater.*, 2011, **21**, 1076–1081.
- 39 S. Na, G. Wang, S.-S. Kim, T.-W. Kim, S. Oh, B. Yu, T. Lee and D. Kim, *J. Mater. Chem.*, 2009, **19**, 9045–9053.
- 40 M. Vosgueritchian, D. J. Lipomi and Z. Bao, *Adv. Funct. Mater.*, 2012, **22**, 421–428.
- 41 Y. Li, R. Tanigawa and H. Okuzaki, *Smart Mater. Struct.*, 2014, **23**, 074010.
- 42 A. Savva, E. Georgiou, G. Papazoglou, A. Z. Chrusou, K. Kapnisis and S. A. Choulis, *Sol. Energy Mater. Sol. Cells*, 2015, **132**, 507–514.
- 43 Y.-Y. Lee, G. M. Choi, S.-M. Lim, J.-Y. Cho, I.-S. Choi, K. T. Nam and Y.-C. Joo, *Sci. Rep.*, 2016, **6**, 25332.
- 44 S.-S. Yoon and D.-Y. Khang, *J. Phys. Chem. C*, 2016, **120**, 29525–29532.
- 45 Y. Wang, C. Zhu, R. Pfattner, H. Yan, L. Jin, S. Chen, F. Molina-Lopez, F. Lissel, J. Liu, N. I. Rabiah, Z. Chen, J. W. Chung, C. Linder, M. F. Toney, B. Murmann and Z. Bao, *Sci. Adv.*, 2017, **3**, e1602076.
- 46 M. Y. Teo, N. Kim, S. Kee, B. S. Kim, G. Kim, S. Hong, S. Jung and K. Lee, *ACS Appl. Mater. Interfaces*, 2017, **9**, 819–826.
- 47 Y. Xia and J. Ouyang, *ACS Appl. Mater. Interfaces*, 2012, **4**, 4131–4140.
- 48 T.-M. Huang, S. Batra, J. Hu, T. Miyoshi and M. Cakmak, *Polymer*, 2013, **54**, 6455–6462.
- 49 K. S. Park, J. Baek, Y. Park, L. Lee, Y.-E. K. Lee, Y. Kang and M. M. Sung, *Adv. Mater.*, 2016, **28**, 2874–2880.
- 50 J. Ouyang, *Displays*, 2013, **34**, 423–436.
- 51 M. Shin, J. H. Song, G.-H. Lim, B. Lim, J.-J. Park and U. Jeong, *Adv. Mater.*, 2014, **26**, 3706–3711.
- 52 A. Manuelli, L. Persano and D. Pisignano, *Org. Electron.*, 2014, **15**, 1056–1061.
- 53 M. Y. Lee, J. Hong, E. K. Lee, H. Yu, H. Kim, J. U. Lee, W. Lee and J. H. Oh, *Adv. Funct. Mater.*, 2016, **26**, 1445–1453.
- 54 Y. Lee, J. Y. Oh, T. R. Kim, X. Gu, Y. Kim, G.-J. N. Wang, H.-C. Wu, R. Pfattner, J. W. F. To, T. Katsumata, D. Son, J. Kang, J. R. Matthews, W. Niu, M. He, R. Sinclair, Y. Cui, J. B.-H. Tok, T.-W. Lee and Z. Bao, *Adv. Mater.*, 2018, **30**, 1704401.
- 55 S. K. Hwang, S.-Y. Min, I. Bae, S. M. Cho, K. L. Kim, T.-W. Lee and C. Park, *Small*, 2014, **10**, 1976–1984.
- 56 J. T. Kim, J. Pyo, J. Rho, J.-H. Ahn, J. H. Je and G. Margaritondo, *ACS Macro Lett.*, 2012, **1**, 375–379.
- 57 J. Yoo, S. Jeong, S. Kim and J. H. Je, *Adv. Mater.*, 2015, **27**, 1712–1717.
- 58 F. Boubée de Gramont, S. Zhang, G. Tomasello, P. Kumar, A. Sarkissian and F. Cicoira, *Appl. Phys. Lett.*, 2017, **111**, 093701.
- 59 H.-C. Chang, C.-L. Liu and W.-C. Chen, *Adv. Funct. Mater.*, 2013, **23**, 4960–4968.
- 60 A. Babel, D. Li, Y. Xia and S. A. Jenekhe, *Macromolecules*, 2005, **38**, 4705–4711.
- 61 C. J. Lin, J. C. Hsu, J. H. Tsai, C. C. Kuo, W. Y. Lee and W. C. Chen, *Macromol. Chem. Phys.*, 2011, **212**, 2452–2458.
- 62 H. Cho, S.-Y. Min and T.-W. Lee, *Macromol. Mater. Eng.*, 2013, **298**, 475–486.
- 63 S.-Y. Min, T.-S. Kim, Y. Lee, H. Cho, W. Xu and T.-W. Lee, *Small*, 2015, **11**, 45–62.
- 64 A. Luzio, E. Canesi, C. Bertarelli and M. Caironi, *Materials*, 2014, **7**, 906–947.
- 65 S. W. Lee, H. J. Lee, J. H. Choi, W. G. Koh, J. M. Myoung, J. H. Hur, J. J. Park, J. H. Cho and U. Jeong, *Nano Lett.*, 2010, **10**, 347–351.
- 66 S. Lee, G. D. Moon and U. Jeong, *J. Mater. Chem.*, 2009, **19**, 743–748.
- 67 J.-C. Lin, W.-Y. Lee, H.-C. Wu, C.-C. Chou, Y.-C. Chiu, Y.-S. Sun and W.-C. Chen, *J. Mater. Chem.*, 2012, **22**, 14682–14690.

- 68 R. L. Andersson, V. Ström, U. W. Gedde, P. E. Mallon, M. S. Hedenqvist and R. T. Olsson, *Sci. Rep.*, 2014, **4**, 6335.
- 69 Y. Lee, S.-Y. Min and T.-W. Lee, *Macromol. Mater. Eng.*, 2017, **302**, 1600507.
- 70 S.-Y. Min, T.-S. Kim, B. J. Kim, H. Cho, Y.-Y. Noh, H. Yang, J. H. Cho and T.-W. Lee, *Nat. Commun.*, 2013, **4**, 1773.
- 71 W. Xu, S.-Y. Min, H. Hwang and T.-W. Lee, *Sci. Adv.*, 2016, **2**, e1501326.
- 72 Y. Lee, T.-S. Kim, S.-Y. Min, W. Xu, S.-H. Jeong, H.-K. Seo and T.-W. Lee, *Adv. Mater.*, 2014, **26**, 8010–8016.
- 73 Y. Lee, S.-Y. Min, T.-S. Kim, S.-H. Jeong, J. Y. Won, H. Kim, W. Xu, J. K. Jeong and T.-W. Lee, *Adv. Mater.*, 2016, **28**, 9109–9116.
- 74 W. Xu, Y. Lee, S.-Y. Min, C. Park and T.-W. Lee, *Adv. Mater.*, 2016, **28**, 527–532.
- 75 H.-S. Ko, Y. Lee, S.-Y. Min, S.-J. Kwon and T.-W. Lee, *Nanoscale*, 2017, **9**, 15766–15772.
- 76 S.-Y. Min, Y. Lee, S. H. Kim, C. Park and T.-W. Lee, *ACS Nano*, 2017, **11**, 3681–3689.
- 77 D. Di Camillo, V. Fasano, F. Ruggieri, S. Santucci, L. Lozzi, A. Camposeo and D. Pisignano, *Nanoscale*, 2013, **5**, 11637–11642.
- 78 Y. Huang, N. Bu, Y. Duan, Y. Pan, H. Liu, Z. Yin and Y. Xiong, *Nanoscale*, 2013, **5**, 12007–12017.
- 79 C. Chang, V. H. Tran, J. Wang, Y.-K. Fuh and L. Lin, *Nano Lett.*, 2010, **10**, 726–731.
- 80 B. Y. Ahn, E. B. Duoss, M. J. Motala, X. Guo, S.-I. Park, Y. Xiong, J. Yoon, R. G. Nuzzo, J. A. Rogers and J. A. Lewis, *Science*, 2009, **323**, 1590–1593.
- 81 B. W. An, K. Kim, H. Lee, S.-Y. Kim, Y. Shim, D.-Y. Lee, J. Y. Song and J.-U. Park, *Adv. Mater.*, 2015, **27**, 4322–4328.
- 82 J.-H. Ahn and J. H. Je, *J. Phys. D: Appl. Phys.*, 2012, **45**, 103001.
- 83 J. T. Kim, S. K. Seol, J. Pyo, J. S. Lee, J. H. Je and G. Margaritondo, *Adv. Mater.*, 2011, **23**, 1968–1970.
- 84 S. K. Seol, W. S. Chang, D. Kim and S. Jung, *RSC Adv.*, 2012, **2**, 8926–8928.
- 85 J. H. Kim, W. S. Chang, D. Kim, S. H. Cho and S. K. Seol, *Mater. Chem. Phys.*, 2014, **147**, 1171–1174.